Available online at www.sciencedirect.com
ScienceDirect
Precambrian Research 151 (2006) 211–223
Precambrian Research
www.elsevier.com/locate/precamres

Hydrothermal alteration at the Panorama Formation, North Pole Dome, Pilbara Craton, Western Australia

Adrian J. Brown [a,*], Thomas J. Cudahy [b,c], Malcolm R. Walter [c]

[a] *SETI Institute, 515 N. Whisman Rd, Mountain View, CA 94043, USA*
[b] *CSIRO Exploration and Mining, ARRC Centre, Kensington, WA 6102, Australia*
[c] *Australian Centre For Astrobiology, Macquarie University, NSW 2109, Australia*

Received 28 April 2006; received in revised form 19 July 2006; accepted 26 August 2006

Abstract

An airborne hyperspectral remote sensing dataset was obtained of the North Pole Dome region of the Pilbara Craton in October 2002. It has been analyzed for indications of hydrothermal minerals. Here we report on the identification and mapping of hydrothermal minerals in the 3.459 Ga Panorama Formation and surrounding strata. The spatial distribution of a pattern of subvertical pyrophyllite rich veins connected to a pyrophyllite rich palaeohorizontal layer is interpreted to represent the base of an acid-sulfate epithermal system that is unconformably overlain by the stromatolitic 3.42 Ga Strelley Pool Chert.
© 2006 Elsevier B.V. All rights reserved.

Keywords: Pilbara; North Pole Dome; Panorama Formation; Pyrophyllite; Hydrothermal; Hyperspectral; Stromatolites; Strelley Pool Chert

1. Introduction

Hyperspectral remote sensing has been used in the past to successfully survey Archean regions of Western Australia (Cudahy et al., 2000). As part of a combined Australian Centre for Astrobiology-CSIRO project to map the North Pole Dome in the Pilbara region, a remote sensing dataset was collected in October 2002 and has been analyzed in the years hence. The dataset was obtained using the reflectance spectrometer called HyMap (Cocks et al., 1998), owned and operated by HyVista Corporation. This instrument measures reflected light from 0.4 to 2.5 μm, and is particularly suited to mapping hydrothermal minerals due to 2.2–2.35 μm vibrational absorptions of the OH^- anion in alteration minerals (Hunt, 1979).

2. Geological setting

The 3.5 Ga Pilbara Craton covers 60,000 km^2 and provides some excellent exposure of low metamorphic grade, relatively undeformed rocks that span much of the Archean (ca. 3.5–2.7 Ga). The Pilbara Craton is divided into three granite-greenstone terranes with distinct geological histories, separated by intervening clastic sedimentary basins (Van Kranendonk et al., 2002). The Pilbara is an important region for investigating early Earth processes, but its state of preservation has also been valuable to investigate processes relevant to all time periods, for example, the study of VHMS systems at the Strelley Granite (Cudahy et al., 2000).

The North Pole Dome (NPD) is located in the center of the East Pilbara Granite Greenstone Terrain (Van Kranendonk, 2000). The NPD is a structural dome of bedded, dominantly mafic volcanic rocks of the Warrawoona and Kelly Groups that dip gently away from the North Pole Monzogranite exposed in the core of the

* Corresponding author. Tel.: +1 650 810 0223.
E-mail address: abrown@seti.org (A.J. Brown).

0301-9268/$ – see front matter © 2006 Elsevier B.V. All rights reserved.
doi:10.1016/j.precamres.2006.08.014

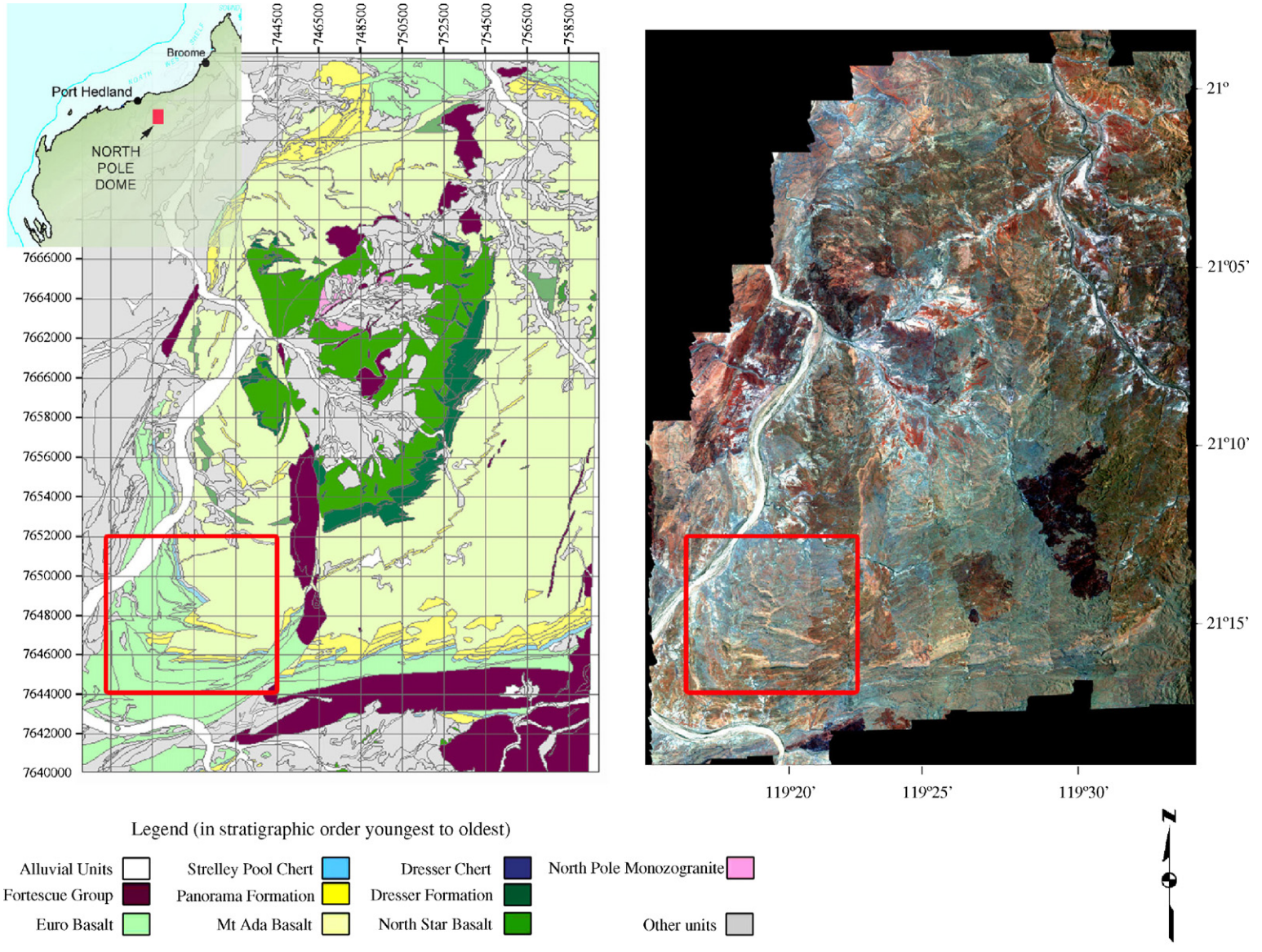

Fig. 1. North Pole Dome with red box outlining the best preserved regions of the Panorama Formation. Grid lines are Australian Map Grid (AMG84 or UTM Zone 50). Each grid box is 2 km across. Mineral maps in Fig. 4 are sourced from the region within the red box.

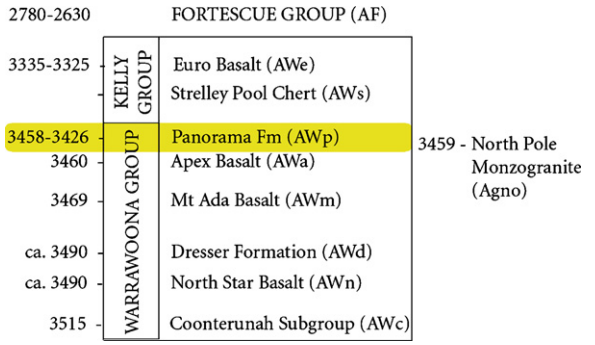

Fig. 2. Stratigraphic column of the geological units within the study region.

Dome (Fig. 1; Van Kranendonk et al., 2002). Average dips vary from 50° to 60° in the inner Dresser Formation to around 30–40° in the outer Panorama Formation (Van Kranendonk, 2000). The North Pole Monzogranite has been estimated to extend ~6 km below the surface by gravity surveys (Blewett et al., 2004). The central Monzogranite has been interpreted as a syn-volcanic laccolith to Panorama Formation volcanic rocks at the top of the Warrawoona Group (Blewett et al., 2004; Van Kranendonk, 1999). Minor outcrops of felsic volcanic rocks are interbedded with the greenstones, and these are capped by cherts that indicate hiatuses in volcanism (Barley, 1993; Van Kranendonk, 2000). An overall arc-related model for hydrothermal activity is favored by Barley (1993), whereas Van Kranendonk has recently supported a mantle-plume driven model for hydrothermal activity at the North Pole Dome (Van Kranendonk, 2006).

A stratigraphic column for the study area (Fig. 2) shows the age and composition of the main stratigraphic units of the Kelly and Warrawoona Groups. Formation codes are given in parentheses. The region is regarded as an important witness to Earth's earliest biosphere since stromatolite and possible microfossil occurrences have been documented at three distinct stratigraphic levels at the NPD—within the Dresser Formation, the Mount Ada Basalt and the Strelley Pool Chert (Dunlop et al., 1978; Walter et al., 1980; Awramik et al., 1983; Ueno et al., 2001; Buick, 1990; Van Kranendonk, 2006; Ueno et al., 2004).

2.1. Warrawoona Group—Panorama Formation (AWp)

The Panorama Formation consists of felsic volcanic rocks that outcrop as a prominent ridge line around the outer part of the NPD. It is up to 1 km thick and has been extensively silicified (Cullers et al., 1993). It has been directly dated (using U–Pb in zircon) as between 3.458 and 3.426 Ga (Van Kranendonk et al., 2002). The rhyolitic Panorama Formation was erupted after the Mt. Ada ultramafic-mafic sequence and Apex Basalt. The variation in style from ultramafic through mafic to felsic volcanics at the NPD was possibly driven by a mantle plume that also drove hydrothermal activity during this period (Van Kranendonk et al., 2006). Remnants of the felsic volcanic rocks of the Panorama Formation are distributed 7–16 km from the center of the North Pole Dome. Some of the most accessible Panorama Formation elements lie in an 8 km × 8 km region on the southwest corner of the Dome, and these make up the study region of this paper.

2.2. Kelly Group (AK)—Strelley Pool Chert (AKs)

The Strelley Pool Chert (SPC) is a marker unit that crops out in greenstone belts across the East Pilbara (Van Kranendonk, 2000). It chiefly consists of a laminated grey to black and white chert that represents silicified carbonate, commonly with coniform stromatolites. It has not been directly dated, but was deposited between 3.426 and 3.335 Ga, the ages of underlying and overlying felsic volcanic rocks (Van Kranendonk, 2006). In the study region, it unconformably overlies the Panorama Formation.

2.2.1. Relationship of Panorama Formation to central NP Monzogranite

Palaeocurrent evidence from crossbedded arenites in the Panorama Formation suggest sediment dispersal from a felsic source close to the modern day center of the NPD (DiMarco, 1989). It has recently been suggested that an eruptive vent of this felsic volcanic source is preserved in the north western part of the NPD (Van Kranendonk, 1999). Van Kranendonk (1999) opined that the NP Monzogranite fed the 'Panorama Volcano' based on similar ages (Thorpe et al., 1992) and the presence of radially oriented dykes leading from the granite to the level of the Panorama Formation (Van Kranendonk, 2000).

2.2.2. Hydrothermal activity associated with the Panorama Formation

Following deposition of the Mt. Ada Basalt, and during or soon after the deposition of the Panorama Formation, an intense period of hydrothermal alteration occurred at the palaeosurface (probably in a shallow submarine setting). A highly schistose, intensely altered, golden brown pyrophyllite-rich horizon represents the alteration event (Van Kranendonk and Pirajno, 2004) that extends around the edge of the NPD, in the contact between the Mount Ada Basalt and the Panorama

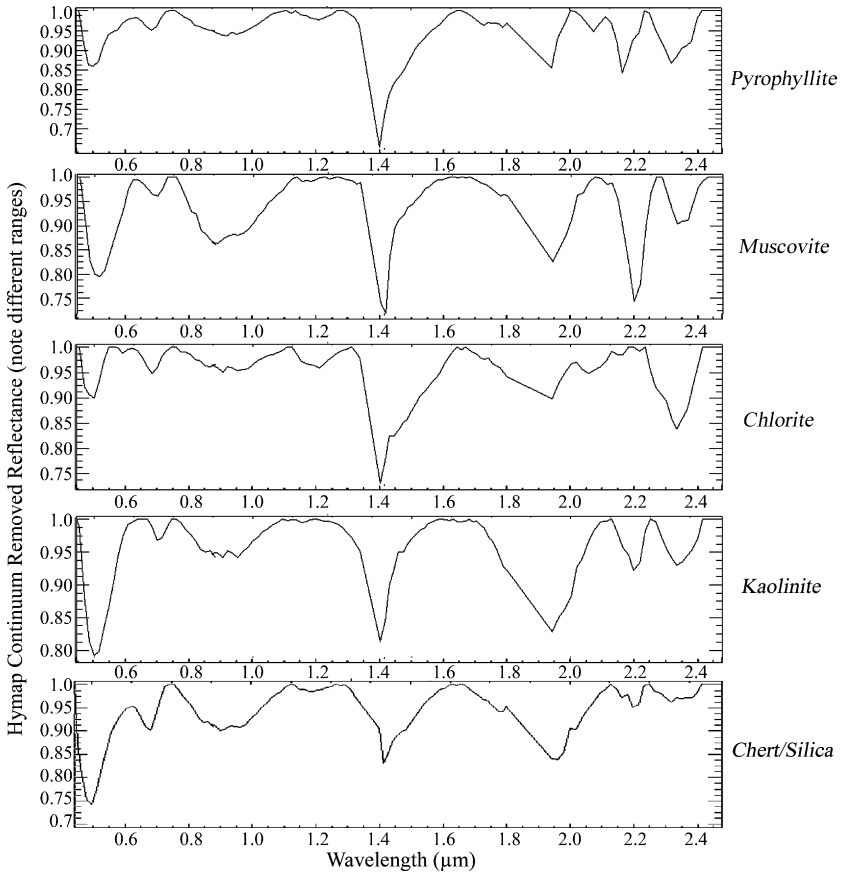

Fig. 3. Representative HyMap continuum removed reflectance spectra for OH-bearing minerals and silica taken from the hyperspectral dataset of the study region.

Formation, and in and adjacent to granite dykes radiating out from the North Pole Monzogranite.

The hydrothermal event and subsequent deformation that gave rise to the pyrophyllite schists in the Mt. Ada Basalt and Panorama Formation predates deposition of the Kelly Group, as the former are affected by a penetrative schistosity and high temperature alteration that is absent from the unconformably overlying rocks of the Kelly Formation (Van Kranendonk and Pirajno, 2004; Brown et al., 2004). The top of the alteration system, as well as structurally higher parts of the alteration system may have been eroded away before emplacement of the overlying Kelly Group—in the form of the downcutting SPC.

3. Remote sensing of hydrothermal minerals and alteration zones

3.1. Detection of vibrations due to OH^-

Electromagnetic radiation that intercepts the surface of a mineral bearing the OH^- cation (often called 'alteration' or hydrothermal minerals) will be absorbed at certain wavelengths due to sympathetic vibrations within the crystal lattice (Hunt, 1977). The electronic neighborhood of the OH^- cation affects the energy of the vibration, and hence the central absorption wavelength, of the reflected light. In this manner, Al–OH bonds in muscovite, for example, can be unequivocally distinguished from Mg–OH bonds in chlorites or amphiboles. Photons with wavelengths between 2.0 and 2.5 μm have similar energies to combinations of fundamental OH^- vibrations, and thus are suitable for detecting hydrothermal minerals.

Fig. 3 shows an example of HyMap spectra of five different minerals. The 2.0–2.5 μm region of each of these spectra is unique and diagnostic of the first four minerals. Silica, the last mineral, is identified by an absence of strong bands in this region. Field mapping has shown this to be a successful strategy in this highly silicified granite-greenstone region. This strategy should be used with caution in other regions, where silicification and alteration minerals are rare, since it does not discriminate between silica and unaltered feldspar or pyroxene,

Table 1
Alteration zones and associated minerals in the Panorama region

Mineral	Alteration Zone			
	Phyllic	Advanced Argillic	Propylitic	Silicic
Muscovite	■			
Pyrophyllite		■		
Chlorite			■	
Silica/Chert				■

for example. Each of the spectra in Fig. 3 has been 'continuum removed' in order to highlight the absorption bands (Clark et al., 1987).

In order to map the diagnostic absorption bands, a computer algorithm has been developed to fit Gaussian-type curves to the absorption bands in the 2.0–2.5 μm region. This process is discussed in more detail in companion papers (Brown et al., 2005; Brown, 2006a). We used the IDL programming language and the ENVI environment (www.rsi.com) to produce mineral maps of hydrothermal minerals with diagnostic absorption bands. Each hydrothermal mineral has been chosen as representative of an alteration zone type on the basis that it is the spectrally dominant contributor to the mineral assemblage (Thompson and Thompson, 1996). The alteration zones and mineral assignments are given in Table 1.

3.2. Al–OH absorption band wavelength

The central wavelength of vibrational absorption bands is very sensitive to the local chemical bonding environment. The central wavelength of the 2.2 μm Al–OH vibration absorption band can be used as a proxy for Al-content in white micas, such as muscovite (Duke, 1994). It has been used to track fluid pathways in hydrothermally altered rocks (van Ruitenbeek et al., 2005) and as a measure of metamorphic grade in muscovitic schists (Longhi et al., 2000). Long wavelength white micas have lower Al content (higher Si content) and short wavelength white micas have higher Al content.

4. Field sampling

Three field trips to the Panorama Formation region from 2003 to 2005 yielded over 85 samples, which have been used to ground-truth hyperspectral mineral maps presented herein (Fig. 4). All major units (including the Euro Basalt, Mt. Ada Basalt, Panorama Formation and Al-rich and poor muscovite veins) in the study area were sampled, particularly those units which displayed spectral heterogeneity. Sample locations are shown on the geological map in Fig. 4. The results of XRD, XRF, IR and EMP analyses of these samples are discussed elsewhere (Brown, 2006b). Hyperspectral mineral identifications were confirmed using petrographic slides, in particular for the identification of the endmember minerals silica, pyrophyllite, muscovite and chlorite. Muscovite was distinguished from pyrophyllite using XRD of small amounts of powdered samples. Al-rich and Al-poor muscovite were distinguished using EMP analysis.

We used a PIMA SWIR hand-held spectrometer (www.hyvista.com) to obtain laboratory IR spectra of all our samples (Brown et al., 2004). These laboratory spectra were used to compare the spectral signature of samples to the signatures of hydrothermal minerals in the airborne dataset.

5. Results

Mineral maps are presented in Fig. 4, along with a 'hydrothermal facies' map where individual mineral maps are combined. A geological map of the region showing sample locations is also provided.

❶ *Intense kaolinite in the Shaw River*: The dry, dusty and sandy river bed of the Shaw River is easily discriminated by its consistent kaolinite signature. Using a kaolinite index linked to the sharpness of the 2.16–2.2 μm doublet of kaolinite (Brown, 2006a, 2006b) suggests that kaolinite in the Shaw River is detrital, and probably due to weathering of felsic Al-rich material from nearby granites and phyllosilicate bearing sandstones.

❷ *Arcuate regions of phyllic alteration*: Phyllic alteration (defined here by the presence of muscovite; Table 1) has two styles in this region: (1) long, thin arcs of ridge-forming "bedding parallel" phyllic alteration follow the general outline of ridges and (2) long thin veins leading up to the arcuate ridges have zones of phyllic alteration. There is a large amount of phyllic alteration on the extreme west of the study area, due to sandstone units of the Gorge Creek Supergroup, which lies outside the NPD (Fig. 4).

❸ *Pervasive propylitic alteration beneath and above the Panorama Formation*: Propylitically altered, chlorite-bearing pillow basalts of the Mt. Ada Basalt and overlying Euro Basalt make up most of the study area. The Euro Basalt has experienced only low strain, low temperature (i.e. propylitic) hydrothermal alteration and very low metamorphic grade (Van Kranendonk, 2000).

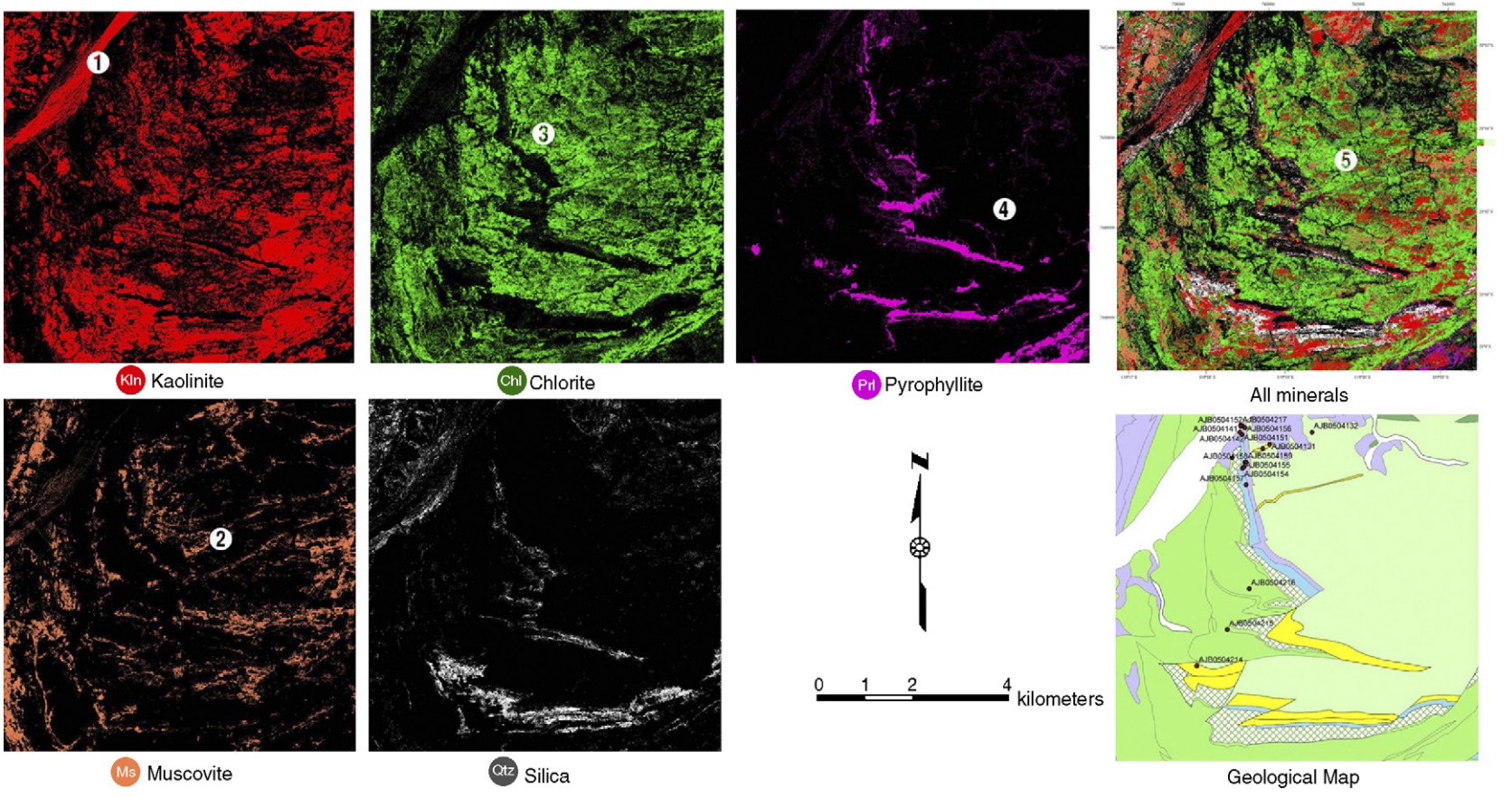

Fig. 4. Mineral maps of the study region, showing distributions of the indicated minerals. See Fig. 1 for coverage. The upper right image is a complete hydrothermal zone map, formed by combining the other five other maps together. Some points are obscured—pyrophyllite was laid down first, then silica, then chlorite, then kaolinite, then muscovite. This is an alteration class map—pink is the phyllic zone, white silicic, red argillic, green propylitic and purple advanced argillic. Part of the geological map from Fig. 1 is provided (Van Kranendonk, 2000) of the region showing sample locations—this shows a silica-rich region of the SPC in hatched green.

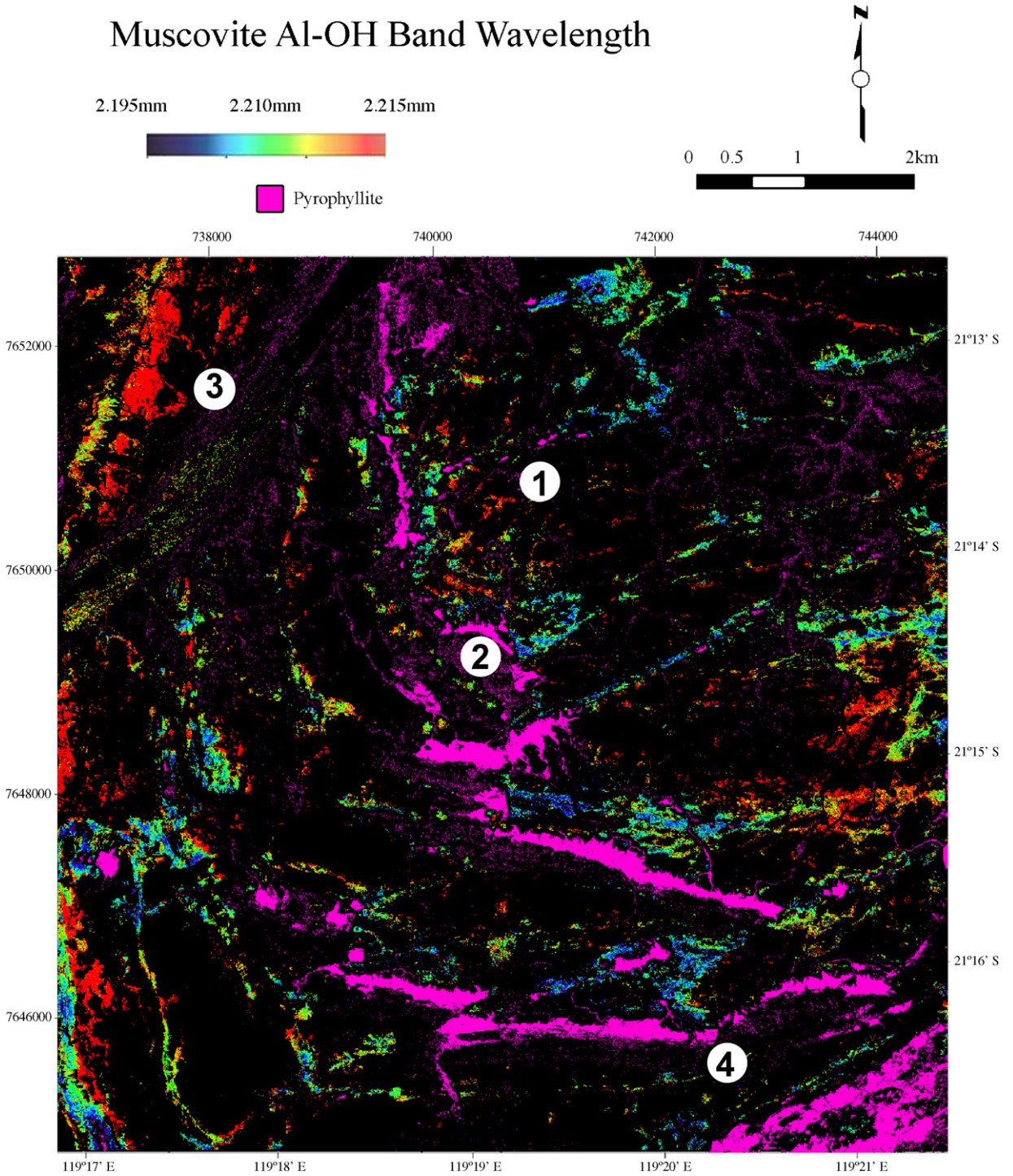

Fig. 5. Muscovite Al–OH wavelength map for the Panorama region. Long wavelength (Al-poor) muscovite is in red and short wavelength (Al-rich) muscovite is in blue. Pyrophyllite is in pink. The area covered is identical to the maps in Fig. 4.

❹ *Advanced argillic alteration*: The determining feature of the Panorama hydrothermal event is the advanced argillic layer defined by the presence of pyrophyllite. Pyrophyllite is largely developed in at least two rock types—the felsic Panorama Formation and the top parts of the underlying mafic Mt. Ada Basalt. Pyrophyllite bearing units outcrop beneath, and do not extend into, the overlying Euro Basalt, indicating that

the timing of the pyrophyllite development was prior to the Euro Basalt deposition. The pyrophyllite bearing units are characterized by highly schistose, golden brown weathering habit. This alteration style was previously interpreted as representing medium temperature (300 °C), alteration with a high strain event during, or soon after, emplacement (Van Kranendonk and Pirajno, 2004).

❺ *Juxtaposition of hydrothermal zones*: Pyrophyllite rich alteration is everywhere developed below the SPC. In addition, it should be noted that the phyllic alteration at the base of veins leading up to the SPC grades from muscovite to pyrophyllite rich, as discussed below.

5.1. Muscovite Al–OH wavelength map

As discussed earlier, white mica Al content can be mapped by tracking the central wavelength of the Al–OH feature near 2.2 μm (Duke, 1994). Using computer algorithms discussed elsewhere (Brown, 2006a), we have generated a muscovite Al–OH wavelength map and overlain the pyrophyllite mineral map (Fig. 5).

❶ *Variations in Al content of white micas beneath pyrophyllite in Panorama Formation*: Around point ❶ in Fig. 5, red colors indicate the presence of long wavelength (Al-poor) white mica just beneath the Panorama Formation. Moving east, linear muscovite veins are represented by progressively bluer colors, indicating a shift to shorter wavelength (Al-rich) muscovite. This pattern also repeats on the extreme east of the map, where red Al-poor veins grade to green and blue Al-rich muscovite. This pattern is not entirely uniform, there are, for example, blue patches of Al-rich muscovite beneath the Panorama Formation (one Al-rich vein terminates near ❷) that display fairly constant blue color.

❷ *Pyrophyllite-rich sub-horizontal zones of the Panorama Formation*: Overall, the muscovite veins described above tend to start Al-rich (blue) in the east, and become more Al-poor (red), and then merge into pyrophyllite sub-vertical veins which then connect with pyrophyllite-rich sub horizontal zones. In most regions, immediately below the pyrophyllite, there is a thin sub-horizontal layer of Al-rich (blue) muscovite, for example at point ❷. This thin horizontal blue layer somewhat hides the nature of the muscovite and pyrophyllite mixing in the veins.

❸ *Gorge Creek Supergroup alteration*: On the extreme left edge of the image, running north-south, a fault zone divides the phyllic alteration of the Gorge Creek Supergroup on the west side from the Euro Basalt (bearing no muscovite) on the right. The younger rocks in the west display well developed phyllic alteration (almost 1 km wide in places) with variations in white mica Al-content from base to top (see also western edge and south west corner of this image).

❹ *Pyrophyllite indicating structural doubling of Panorama Formation*: In the bottom of Fig. 5, the occurrence of pyrophyllite is showing the structural faulting and doubling of the same horizon. The patch of pyrophyllite in the south east corner represents a larger exposure of the Panorama Formation controlled by the north-south trending Antarctic Fault which cuts through the NPD (Van Kranendonk, 2000). As can be seen by comparing it to the Van Kranendonk's geological map in Fig. 4, this horizon was not mapped by him—it has been interpreted previously as Euro Basalt. The structural repetition of the Panorama Formation in the south of the study area is also shown on the pyrophyllite mineral map (Figs. 4 and 5).

6. Discussion

6.1. Background propylitic alteration

The mafic pillow rocks of the underlying Mt. Ada Basalt have all been extensively altered to chlorite–carbonate, possibly via the reaction described by Eq. (1) in Table 2. The presence of hydrothermal chlorite unfortunately does not uniquely distinguish them amongst the chloritically altered basalts present throughout the Warrawoona Group and in the overlying Kelly Group (Fig. 2, to the left of point ❸).

6.2. Heat source for the Panorama hydrothermal event

Van Kranendonk and Pirajno (2004) suggested that the heat source that drove silicic hydrothermal alteration of the SPC and Panorama Formation was the thick komatiitic basalt of the Euro Basalt on top of the SPC. This scenario seems unlikely following this study, given the presence of thin (but spatially extensive), relatively unaltered and unfoliated erosional units wedged in various locations in the study area between the pyrophyllite unit and the SPC. The similar alteration style in muscovite bearing veins leading up to the pyrophyllite layer suggests that the phyllic and pyrophyllite alteration was generated by a subvolcanic heat source, specifically the North Pole Monzogranite. What is not clear is how far below the palaeosurface the pyrophyllite layer was developed and how much of the top part of the system (including possible sinters, vents and exhalative miner-

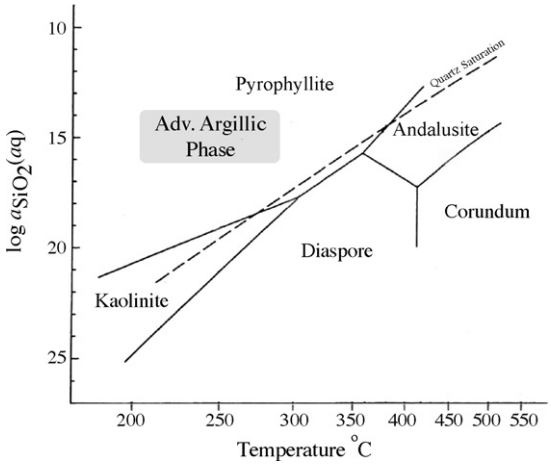

Fig. 6. Phase diagram of the Al_2O_3–SiO_2–H_2O system at 1–2 kbar after (Hemley et al., 1980).

alization which have not been found to date) has been eroded away prior to the unconformity at the base of the Kelly Group.

6.3. Occurrence of pyrophyllite

Pyrophyllite is a rock-forming mineral that occurs in a limited range of metamorphic and hydrothermal conditions. The primary condition for its petrogenesis is high Al—more Al than can be accommodated by the relatively aluminous alteration minerals muscovite, chlorite, chloritoid and lawsonite (Evans and Guggenheim, 1988). It commonly occurs in rocks that are enriched (relatively) in Al through base leaching during hydrothermal alteration, and is precipitated in hydrothermal veins (Evans and Guggenheim, 1988). It appears in both these circumstances in the Panorama Formation.

The phase diagram for the Al_2O_3–SiO_2–H_2O system is shown in Fig. 6 (Hemley et al., 1980). This shows the control that high silica fluids have over whether pyrophyllite or kaolinite is precipitated from this system at

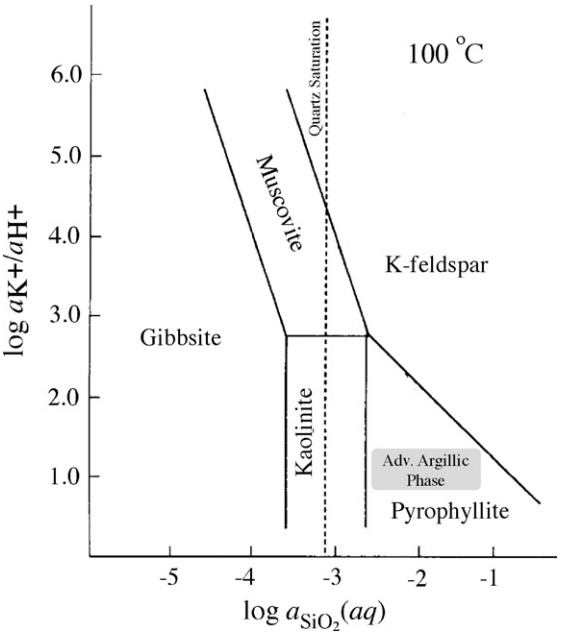

Fig. 7. Activity diagram of $\log a_{K^+}/a_{H^+}$ vs. silica content at 100 °C. Generated using computer code SUPCRT92 after (Johnson et al., 1992).

low temperature. In fluids with high amounts of dissolved silica, pyrophyllite is the preferred phase.

The activity diagram of activity of K^+/activity of H^+ versus silica content for the Al_2O_3–SiO_2–H_2O system is shown in Fig. 7 (Johnson et al., 1992). This diagram was generated using the SUPCRT92 computer code (Johnson et al., 1992). The diagram shows that in high silica and low pH conditions, pyrophyllite will be formed in preference to kaolinite.

Combining information from Figs. 6 and 7, at near surface conditions (100 °C and 1 atm) pyrophyllite is more stable than kaolinite (and muscovite) in waters supersaturated in silica (Hemley et al., 1980). The occurrence of pyrophyllite at the top of sub-vertical muscovite veins may indicate a drop in temperature, a drop in oxy-

Table 2
Probable hydrothermal alteration reactions, temperatures and conditions to produce observed mineral assemblages in the Panorama Formation region

Equation no.	Hydrothermal zone	Chemical reaction	Temperature (°C)	Conditions	Reference
1	Propylitic or greenschist	$5Mg^{2+} + \underset{\text{anorthite}}{CaAl_2Si_2O_8} + 8H_2O + SiO_2 \Rightarrow \underset{\text{chlorite}}{Mg_5AlSi_3AlO_{10}(OH)_8} + Ca^{2+} + 8H^+$	100–200		Hemley et al. (1980)
2	Phyllic	$3\underset{\text{k-fspar}}{KAlSi_3O_8} + H^+ \Leftrightarrow \underset{\text{muscovite}}{KAl_2(Si_3Al)O_{10}(OH)_2} + 6\underset{\text{quartz}}{SiO_2} + K^+$	100–300	pH > 2	Montoya and Henley (1975)
3	Advanced argillic	$2\underset{\text{muscovite}}{KAl_2(Si_3Al)O_{10}(OH)_2} + 6SiO_2 + 2H^+ \Leftrightarrow 3\underset{\text{pyrophyllite}}{Al_2Si_4O_{10}(OH)_2} + 2K^+$	100 or 200–300	pH ∼ 2	Evans and Guggenheim (1988)

gen fugacity or an increase in silica content in the fluids or wall rock.

6.4. pH conditions of the hydrothermal system

One possible explanation for the observed mineral variation is that acidic CO_2-rich vapor was released as the fluids ascended and decompressed, attacking and altering the upper parts of the system to an advanced argillic stage whereas the lower parts remained at the phyllic stage (White and Hedenquist, 1990). Chemical Eqs. (2) and (3) in Table 2 provide a possible pathway for the coexistence of muscovite and pyrophyllite in this system. In more acidic, silica-rich parts of the system, pyrophyllite is favored over muscovite. In less acidic conditions, muscovite predominates.

6.5. Redox conditions of the Panorama hydrothermal system

Recent research at the CSIRO Division of Exploration and Mining suggests pyrophyllite may be preferred to kaolinite or muscovite in reducing acidic conditions (J. Walshe, personal communication). It is possible that a reducing ocean may have been the source of hydrothermal fluids in the top, pyrophyllite rich part of the Panorama hydrothermal system (Nakamura and Kato, 2004).

6.6. Silica content of hydrothermal fluids

A final factor controlling the deposition of pyrophyllite and muscovite in the vein systems is the silica content of the fluids. An increase in silica at the paleosurface may have been driven by a high silica Archean ocean (Knauth and Lowe, 2003). Silica-rich water drawn down into the top reaches of the hydrothermal system may have allowed the precipitation of pyrophyllite in preference to muscovite. The highly siliceous Panorama Formation may also have been a source of silica in the veins of this hydrothermal system.

6.7. Panorama hydrothermal event as an acid-sulfate system

An acid-sulfate type system is favored to describe the Panorama hydrothermal event primarily due to the intense advanced argillic alteration, driven by acidic, reducing fluids, which is consistent with the preserved mineral assemblages.

The muscovite-altering-to-pyrophyllite patterns in Fig. 5 provide evidence for a change in fluid chemistry within the deep penetrating (1–4 km) sub-vertical veins. The clear connection of pyrophyllite and muscovite in these veins, and the variations of these two minerals suggests a genetic link between the sub vertical and sub horizontal zones of the Panorama Formation, with alteration styles changing across-strike (up stratigraphy) due to temperature, acidity or redox conditions in a continuously connected hydrothermal system approaching the paleosurface.

It is possible the pyrophyllite alteration of the Panorama event occurred in low temperature (100 °C) conditions (Gradusov and Zotov, 1975). Temperature is not a well constrained parameter of acid-sulfate systems (Heald et al., 1987). It is of note that salinities of acid-sulfate systems are commonly quite high (usually 5–24% NaCl equivalent, Hayba et al., 1985). An important alteration mineral in acid-sulfate systems is alunite—this has not been found in this study, though it was reported by Van Kranendonk and Pirajno (2004) in the Strelley Pool Chert level. Identification of characteristic minerals, such as alunite and jarosite in future studies would support the moniker of "acid-sulfate" for this hydrothermal system.

7. Petrogenetic model

A three-stage model may best describe the genesis of the rocks within the study region for the development of main geological features in the study area is proposed:

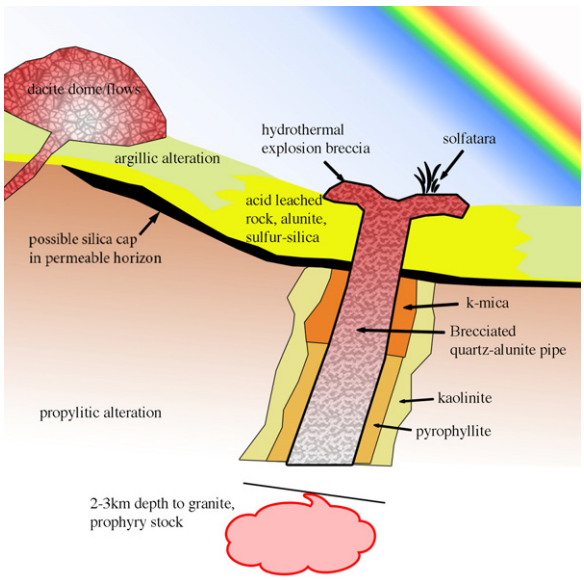

Fig. 8. Schematic cross section of epithermal high sulfur type deposit associated with granodiorite magmatism. From Bonham and Giles (1984).

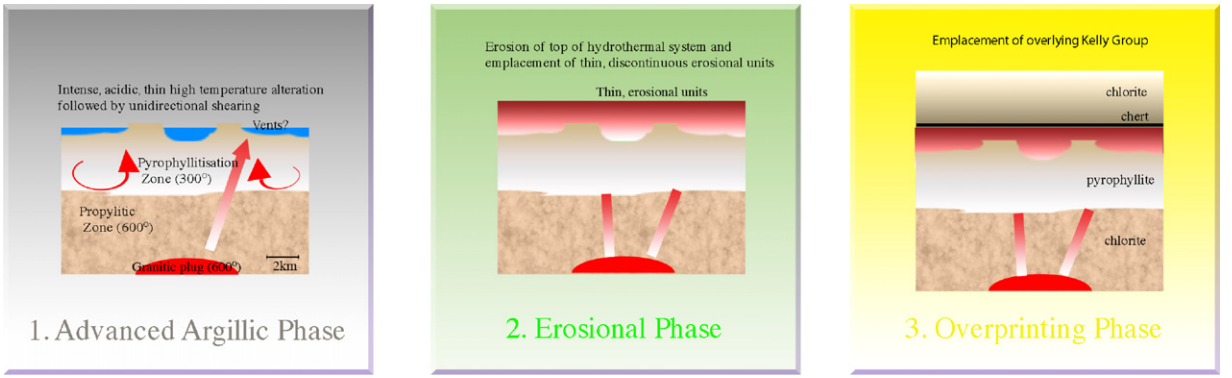

Fig. 9. Genetic model for the study region. See text for discussion.

❶ *Advanced argillic phase*: Following shallow intrusion of the North Pole Dome Monzogranite, quartz porphyry veins were emplaced into the overlying crust and fed surface volcanic rocks of the Panorama Formation. Pertinent features of epithermal ore deposits formed under similar conditions are represented in the schematic diagram shown in Fig. 8 (after Bonham and Giles, 1984). The figure shows a subaerial system, however a shallow marine to occasional subaerial environment has been suggested by REE systematics and eruption patterns of the Panorama Volcano (Van Kranendonk and Hickman, 2000; Bolhar et al., 2005).

❷ *Erosional phase*. Following the deposition of the Panorama Formation and cooling of the magma source, an erosional phase began. It is probable that the upper parts of the Panorama Formation volcanics were lost to erosion, and thin subaerial deposits were then emplaced upon an unconformity, followed by the Kelly Group rocks of the SPC.

❸ *Depositional phase*. The rocks of the Kelly Group were laid down all over the East Pilbara on top of a regional unconformity, trapping and preserving evidence of the Panorama hydrothermal event and thin subaerial erosional units below. The lower parts of the Kelly Group, including the SPC, were extensively silicified, perhaps in low temperature alteration caused by the later eruption of the ultramafic/mafic Euro Basalt.

We therefore propos a genetic model for the Panorama Formation and surrounding units within the study region, which is summarized schematically in Fig. 9.

8. Conclusion

The hyperspectral maps presented here show that pyrophyllite is not limited to the paleosurface, but extends continuously down deep (several km) subvertical veins where muscovite eventually becomes prevalent. This suggests a syngenetic nature between subvertical and paleosurface (or shallow subsurface) pyrophyllite alteration. The remote sensing data favor a model where the veins fed hydrothermal fluids responsible for the pyrophyllite alteration in the horizontal paleosurface and vertical veins.

Acid-sulfate hydrothermal systems typically produce sulfates, such as alunite and jarosite in their surface expressions (White and Hedenquist, 1990). This study has not revealed the location of any associated sulfate minerals, although their presence (even in small abundance) would do much to support the hydrothermal model presented here. If they have not been totally eroded, they would be ideal targets for further exploration in the region of the Panorama Formation.

Acknowledgements

We thank the Geological Survey of Western Australia, particularly Tim Griffin, Brian Moore, Arthur Hickman, Martin Van Kranendonk and Kath Grey, for their generous assistance without which the fieldwork phase of this project would not have been possible. We also thank the GEMOC Analysis Unit, particularly Norm Pearson, Carol Lawson and Tin Tin Win, at Macquarie University for assistance with XRD and EMP measurements.

References

Awramik, S.M., Schopf, J.W., Walter, M.R., 1983. Filamentous fossil bacteria from the Archaean of Western Australia. Precambrian Res. 20, 357–374.

Barley, M.E., 1993. Volcanic sedimentary and tectonostratigraphic environments of the ca. 3.46 Ga Warrawoona Megasequence. Precambrian Res. 60, 69–98.

Blewett, R.S., Shevchenko, S., Bell, B., 2004. The North Pole Dome: a non-diapiric dome in the Archaean Pilbara Craton, Western Australia. Precambrian Res. 133, 105–120.

Bolhar, R., Van Kranendonk, M.J., Kamber, B.S., 2005. A trace element study of siderite-jasper banded iron formation in the 3.45 Ga Warrawoona Group, Pilbara Craton—formation from hydrothermal fluids and shallow seawater. Precambrian Res. 137, 93–114.

Bonham Jr., H.F., Giles, D.L. (Eds.), 1984. Epithermal Gold/Silver Deposits—The Geothermal Connection. Geothermal Resources Council, p. 384.

Brown, A.J., 2006a. Spectral Curve Fitting for Automatic Hyperspectral Data Analysis. IEEE Trans. Geosci. Remote Sensing 44 (6), 1601–1608.

Brown, A.J., 2006b. Hyperspectral mapping of ancient hydrothermal systems. Ph.D. Thesis. Macquarie University.

Brown, A.J., Cudahy, T.J., Walter, M.R., 2004. Short wave infrared reflectance investigation of sites of Palaeobiological interest: applications for Mars exploration. Astrobiology 4, 359–376.

Brown, A.J., Walter, M.R., Cudahy, T.J., 2005. Hyperspectral imaging spectroscopy of a Mars analog environment at the North Pole Dome, Pilbara Craton, Western Australia. Aust. J. Earth Sci. 52, 353–364.

Buick, R., 1990. Microfossil recognition in Archean rocks: an appraisal of spheroids and filaments from a 3500 m.y. old chert-barite unit at North Pole, Western Australia. Palaios 5, 441–459.

Clark, R.N., King, T.V.V., Gorelick, N., 1987. Automatic continuum analysis of reflectance spectra. Proceedings of the Third Airborne Imaging Spectrometer Data Analysis Workshop, JPL Publication 87–30, pp. 138–14.

Cocks, T., Jenssen, R., Stewart, A., Wilson, I., Shields, T., 1998. The HyMap airborne hyperspectral sensor: the system, calibration and performance. In: 1st EARSeL Conference, pp. 37–42.

Cudahy, T.J., Okada, K., Brauhart, C., 2000. Targeting VMS-style Zn mineralization at Panorama, Australia, using airborne hyperspectral VNIR-SWIR HyMap data. In: Environmental Research Institute of Michigan, International Conference on Applied Geologic Remote Sensing, 14th Las Vegas, Nevada, Proceedings, pp. 395–402.

Cullers, R.L., Dimarco, M.J., Lowe, D.R., Stone, J., 1993. Geochemistry of a Silicified, Felsic Volcaniclastic Suite from the Early Archean Panorama Formation, Pilbara Block, Western-Australia—an Evaluation of Depositional and Postdepositional Processes with Special Emphasis on the Rare-Earth Elements. Precambrian Res. 60, 99–116.

DiMarco, M.J., 1989. Polytypes of 2:1 dioctahedral micas in silicified volcaniclastic sandstones, Warrawoona Group, Eastern Pilbara Block, Western Australia. Am. J. Sci. 289, 649–660.

Duke, E.F., 1994. Near infrared spectra of muscovite, Tschermak substitution, and metamorphic reaction progress: implications for remote sensing. Geology 22, 621–624.

Dunlop, J.S.R., Muir, M.D., Milne, V.A., Groves, D.I., 1978. A new microfossil assemblage from the Archaean of Western Australia. Nature 274, 676–678.

Evans, B.W., Guggenheim, S., 1988. Talc, pyrophyllite and related minerals. In: Bailey, S.W. (Ed.), Hydrous Phyllosilicates (Exclusive of Micas), Reviews in Mineralogy, vol. 19, pp. 225–294.

Gradusov, B.P., Zotov, A.V., 1975. Low temperature pyrophyllite in surface deposits around acid springs on Kunashir Island, Doklady. Acad. Sci. U.S.S.R. Earth Sci. Sect. 224, 141–143.

Hayba, D.O., Bethke, P.M., Heald, P., Foley, N.K., 1985. Geologic, mineralogic and geochemical characteristics of volcanic-hosted epithermal precious metal deposits. In: Bethke, P.M., Berger, B.R. (Eds.), Geology and Geochemistry of Epithermal Systems, vol. 2, pp. 129–167.

Heald, P., Foley, N.K., Hayba, D.O., 1987. Comparative anatomy of volcanic-hosted epithermal deposits: acid-sulfate and Adularia sericite types. Econ. Geol. 82, 1–26.

Hemley, J.J., Montoya, J.W., Marinenko, J.W., Luce, R.W., 1980. Equilibria in the system Al_2O_3–SiO_2–H_2O and some implications for alteration/mineralization process. Econ. Geol. 75, 210–228.

Hunt, G.R., 1979. Near infrared (1.3–2.4 um) spectra of alteration minerals—potential for use in remote sensing. Geophysics 44, 1974–1986.

Hunt, G.R., 1977. Spectral signatures of particular minerals in the visible and near infrared. Geophysics 42, 501–513.

Johnson, J.W., Oelkers, E.H., Helgeson, H.C., 1992. SUPCRT 92. A software package for calculating the standard molal thermodynamic properties of minerals, gases, aqueous species and reactions from 1 to 5000 bar and 0 °C to 1000 °C. Comput. Geosci. 18, 899–947.

Knauth, L.P., Lowe, D.R., 2003. High Archean climatic temperature inferred from oxygen isotope geochemistry of cherts in the 3.5 Ga Swaziland Supergroup, South Africa. Geol. Soc. Am. Bull. 115, 566–580.

Longhi, I., Mazzoli, C., Sgavetti, M., 2000. Determination of metamorphicgrade in siliceous muscovite-bearing rocks in Madagascar using reflectance spectroscopy. Terra Nova 12, 21–27.

Montoya, J.W., Henley, R.W., 1975. Activity relations and stabilities in alkali feldspar and mica alteration reactions. Econ. Geol. 70, 577–594.

Nakamura, K., Kato, Y., 2004. Carbonatization of oceanic crust by the seafloor hydrothermal acitivty and its significance as a CO_2 sink in the Early Archean. Geochim. Cosmochim. Acta 68 (22), 4595–4618.

Thompson, A.J.B., Thompson, J.F.H., 1996. Atlas of alteration: a field and petrographic guide to hydrothermal alteration minerals. Geological Association of Canada, Mineral Deposits Division.

Thorpe, R.I., Hickman, A.H., Davis, D.W., Mortensen, J.K., Trendall, A.F., 1992. U–Pb zircon geochronology of Archaean felsic units in the Marble Bar region, Pilbara Craton, Western Australia. Precambrian Res. 56, 169–189.

Ueno, Y., Isozaki, Y., Yurimoto, H., Maruyama, S., 2001. Carbon isotopic signatures of individual microfossils from Western Australia. Int. Geol. Rev. 43, 196–212.

Ueno, Y., Yoshioka, H., Maruyama, S., Isozaki, Y., 2004. Carbon isotopes and petrography of kerogens in ~3.5-Ga hydrothermal silica dikes in the North Pole area, Western Australia. Geochim. Cosmochim. Acta 68, 573–589.

Van Kranendonk, M., 2006. Volcanic degassing, hydrothermal circulation and the flourishing of early life on Earth: A review of the evidence from c. 3490–3240 Ma rocks of the Pilbara Supergroup, Pilbara Craton, Western Australia. Earth Sci. Rev. 74, 197–240.

Van Kranendonk, M., 1999. Two-stage degassing of the Archaean mantle: Evidence from the 3.46 Ga Panorama Volcano, Pilbara Craton, Western Australia. GSWA 99 extended abstracts: New geological data for WA explorers: Western Australia Geological Survey Record 1999/6, pp. 1–3.

Van Kranendonk, M., Hickman, A.H., 2000. Archaean geology of the North Shaw region, East Pilbara Granite Greenstone Terrain. Western Australia—a field guide. GSWA.

Van Kranendonk, M., Webb, G.E., Kamber, B.S., 2006. Geological and trace element evidence for a marine sedimentary environment of deposition and biogenicity of 3.45 Ga stromatolitic carbonates in the Pilbara Craton, and support for a reducing Archaean ocean. Geobiology 1, 91–108.

Van Kranendonk, M.J., 2000. Geology of the North Shaw 1:100,000 Sheet. Geological Survey of Western Australia, Department of Minerals and Energy.

Van Kranendonk, M.J., Pirajno, F., 2004. Geochemistry of metabasalts and hydrothermal alteration zones associated with ca. 3.45 Ga chert+/− barite deposits: implications for the geological setting of the Warrawoona Group, Pilbara Craton, Australia. Geochem.: Exploration, Environ. Anal. 4, 253–278.

Van Kranendonk, M.J., Hickman, A.H., Smithies, R.H., Nelson, D.R., Pike, G., 2002. Geology and tectonic evolution of the Archean North Pilbara terrain, Pilbara Craton, Western Australia. Econ. Geol. Bull. Soc. Econ. Geol. 97, 695–732.

van Ruitenbeek, F.J.A., Cudahy, T.J., Hale, M., van der Meer, F., 2005. Tracing fluid pathways in fossil hydrothermal systems with near infrared spectroscopy. Geology 33, 597–600.

Walter, M.R., Buick, R., Dunlop, J.S.R., 1980. Stromatolites 3400–3500 Myr old from the North Pole area, Western Australia. Nature 284, 443–445.

White, N.C., Hedenquist, J.W., 1990. Epithermal environments and styles of mineralization: variations and their causes, and guideline for exploration. J. Geochem. Exploration 36, 445–474.